In-situ, real-time monitoring of thermo-mechanical properties of biological tissues undergoing laser heating and ablation

Bayan Kurbanova, Shakhrizat Alisherov, Zhannat Ashikbayeva, Zhanerke Katrenova, Akbota Sametova, Abduzhappar Gaipov, Carlo Molardi, Wilfried Blanc, Daniele Tosi, Zhandos Utegulov

Research Article Vol. 15, No. 11 / 1 Nov 2024 / Biomedical Optics Express 6198
Biomedical Optics EXPRESS

In-situ, real-time monitoring of thermo-mechanical properties of biological tissues undergoing laser heating and ablation

BAYAN KURBANOVA,[1,*] SHAKHRIZAT ALISHEROV,[2] ZHANNAT ASHIKBAYEVA,[2,3] ZHANERKE KATRENOVA,[2] AKBOTA SAMETOVA,[2] ABDUZHAPPAR GAIPOV,[4] CARLO MOLARDI,[2] WILFRIED BLANC,[5] DANIELE TOSI,[2,3] AND ZHANDOS UTEGULOV[1]

[1]*Department of Physics, School of Sciences and Humanities, Nazarbayev University, 010000 Astana, Kazakhstan*
[2]*Department of Electrical and Computer Engineering, School of Engineering and Digital Sciences, Nazarbayev University, 010000 Astana, Kazakhstan*
[3]*Laboratory of Biosensors and Bioinstruments, National Laboratory Astana, 010000 Astana, Kazakhstan*
[4]*Department of Medicine, Nazarbayev University School of Medicine, 010000 Astana, Kazakhstan*
[5]*Université Côte d'Azur, INPHYNI, CNRS UMR7010, 17 rue Julien Lauprêtre, 06200 Nice, France*
[*]*bayan.kurbanova@nu.edu.kz*

Abstract: In this work, Brillouin light-scattering spectroscopy and optical backscattering reflectometry (OBR) using Mg–silica-NP-doped distributed sensing fibers were employed for monitoring local GHz visco-elastic properties and surface temperature, respectively, *during* laser driven heating and ablation of chicken tissues. The spatial temperature distribution measured by OBR at various infrared laser heating powers and times was used to validate spatio-temporal local temperature variations modeled by the finite element method via solving Pennes' bioheat conduction equation. The reduction of viscosity and stiffness in chicken skin during its laser heating was attributed to water loss, protein denaturation and change in lipid phase behavior. These findings open avenues for the simultaneous real-time hybrid optical sensing of both viscoelasticity and local temperature in biological tissues undergoing denaturation and gelation during thermal ablation in clinical settings.

1. Introduction

In contemporary medical interventions, thermal therapy stands out as a highly effective alternative to surgery. The primary goal of thermal therapy is to deliberately alter the temperature of tissues in a specific area over a period, prompting a desired biological response [1]. On implementing different thermal therapies (radiofrequency, microwaves and etc.), the existing surgical method consistently faces challenges like insufficient imaging techniques, suboptimal power delivery for creating an effective ablation zone, and difficulty in generating a large enough ablation area for treating sizable tumors. These limitations hinder the precise creation of coagulation zones, making it challenging to target a volume that adequately covers the tumor without impacting the surrounding safe region. Moreover, complications like burns to nearby organs or the bile duct frequently arise due to excessive heat transmission [2]. These issues are critical for patients as tumors tend to reappear from inadequately cauterized areas. Therapies employing ablative lasers present promising advantages including quicker procedures, reduced tissue damage, minimized bleeding, faster recovery, and decreased scarring. These attributes position them as a hopeful approach in cancer treatment. Laser-induced thermal therapy (LITT) holds considerable importance across various oncology practices, serving as an alternative to traditional surgical procedures, particularly beneficial for patients unsuitable for surgery [1]. Laser ablation works on

#537374 https://doi.org/10.1364/BOE.537374
Journal © 2024 Received 22 Jul 2024; revised 7 Sep 2024; accepted 7 Sep 2024; published 4 Oct 2024

Biomedical Optics EXPRESS

the principle of converting absorbed laser light into heat in tissue, resulting in coagulative necrosis. Especially, lasers operating in the infrared (IR) wavelength range possess higher absorption properties by water compared to lasers of other wavelengths. LITT stands as a percutaneous method for ablating tumors by utilizing high-power lasers inserted into the tumor interstitially. This approach administers thermal therapy guided by MRI, inducing tumor ablation through coagulation necrosis [3,4]. Research findings highlight its effectiveness not just in treating pediatric brain tumors [5] but also in addressing small, palpable invasive breast carcinomas [6].

The skin, being the body's largest organ, can be seen as a three-tiered system comprising the epidermis, dermis, and subcutis. Temperature variations within skin tissue occur unevenly due to factors such as internal heat production, temporal and spatial heat sources and drains, as well as heat transfer between the skin's surface and the surrounding external environment. Comprehending how lasers ablate skin tissue, could offer valuable insights for assessing burn injuries [7] and treating cancer through hyperthermia [8]. Yet, many current approaches concentrate solely on temperature measurements to estimate the extent of tissue affected by applied heat, often overlooking or underestimating the thermo-mechanical changes occurring during this process.

Skin bio-thermomechanics, a deeply interdisciplinary field, is formed to explore the interconnected thermal, mechanical, and biological reactions within skin tissue [9]. When heated, the thermal alteration of collagen causes mechanical stress, leading to substantial shrinkage at a larger scale. Beyond structural modifications, collagen hydration shifts during denaturation, potentially releasing water initially and absorbing it later. As expected, the thermal denaturation of collagenous tissue can bring about significant modifications in its viscoelastic characteristics [10]. Practically all biological materials, including hard tissues, exhibit mechanical viscoelasticity due to the presence of viscoelastic components in their extracellular matrices, tissue cells, and structural proteins [11]. Investigations into the temperature-dependent viscoelastic properties of collagen-based tissues like cartilage and bone have revealed that their viscoelastic behavior is significantly influenced by the amount of water they contain [12,13]. Differential scanning calorimetry and dynamic mechanical analyzer techniques were used to study dynamic viscoelastic properties of pig skin tissue and it was shown that the storage modulus is temperature sensitive, but the loss factor does not show a significant dependency on either temperature or thermal denaturation [10].

Thermal deformation and stresses are always coupled with heat transfer, and even a slight change in heat-induced stress can trigger a sensation of pain in biological tissues, similar to the effect of temperature [14]. Numerous studies have utilized analytical methods to solve Pennes' bioheat transfer equation, given its simplicity under specific conditions [9,15]. Numerical investigations into the transient thermoviscoelastic behaviors of layered tumors have highlighted the significant influence of temperature-dependent thermal conductivity on both thermal and mechanical responses during hyperthermia treatment [16]. An analytical approach employing Laplace transformation has been introduced to determine thermal damage and temperature changes in living tissue resulting from laser irradiation [17]. Although informative, the current theoretical modeling has certain constraints, with a primary limitation being the assumption of constant properties in skin tissue, owing to the scarcity of relevant experimental studies. Additional experiments are required to enhance our comprehension of property variations with temperature and the associated collagen denaturation. This knowledge is essential for the development of more advanced models in the future. However, measuring the bio-thermomechanical behavior of skin tissue under physiological conditions is technically challenging.

Brillouin light scattering (BLS) micro-spectroscopy relies on laser light that is scattered inelastically by thermally excited GHz acoustic waves within a probed dense medium. This optical technique is non-invasive and non-contact and can probe visco-elastic properties of studied media with micro-scale spatial resolution. BLS spectroscopy has found applications in

Biomedical Optics EXPRESS

soft matter and materials science studies [18,19], geosciences [20], biomedical research [21–23] and biomarker detection [24–26], including probing of tissue biomechanics at a micrometer scale, paving the way for live cell imaging [27,28].

Regarding localized optical temperature measurement, the OBR method emerges as the most contemporary approach using fiber-optic sensors (FOS) during thermal ablation with millimeter spatial resolution. Specifically, Mg–silicate-NP-doped fibers exhibit stronger backscattering signals compared to standard single-mode fibers. This extension of OBR enables real-time tracking of temperature distribution across the inner layer of thermal ablation, presenting a valuable alternative to thermal imaging with simpler execution [29]. Chaotic attractors, contingent on optical transmittance, offer an experimental means to monitor thermal alterations in photodamaged biological samples [30]. Local viscoelastic variations and temperature change of radiofrequency (RF) post-heated and post-ablated chicken muscle and bovine liver tissues were measured by integrating BLS and OBR techniques [31]. The possibility of combining real-time BLS analysis with distributed 2D thermometry exploiting distributed sensing can serve as an investigative tool for the aforementioned thermal ablation procedures, but most significantly it can be applied as a direct measurement of the tissue properties in superficial and shallow-seated tumors. Shauffer [32] reviewed possible applicative contexts for thermo-therapies in shallow-seated tumors, such as breast carcinoma and chest wall-located tumors. Other tumors localized at the skin level that have been treated with thermo-therapies include superficial bladder carcinoma [33], and non-melanoma skin cancers [34].

In this work, we report for the first time the hybrid application of BLS micro-spectroscopy with OBR for *in-situ* monitoring of local viscoelasticity and temperature within chicken skin *during* its laser-induced heating and ablation at different IR incident laser powers and heating times. The distributions of Mg–silicate-NP-doped sensing fibers along tissue during ablation allowed for the planar measurement of the local temperature profile and assessment of the laser-ablated zone. This measured spatial temperature distribution for different IR laser powers and heating times was utilized to validate temperature distribution obtained via solving Penne's bio-heat conduction equation [35] using finite-element mesh (FEM) approach. The viscoelastic property variation extracted from temperature- and time-dependent spectral Brillouin peak shifts and linewidths in tissues with thermal lesions was studied in correlation with respective spatio-temporal temperature variations during laser-induced heating and ablation processes.

2. Materials and methods

Brillouin spectra were recorded using a 6-pass tandem Fabry–Perot Interferometer TFP-2 (Table Stable Ltd., Mettmenstetten, Switzerland) in the 180°- backscattering setup. The setup's free spectral range was adjusted to 25 GHz. A 532 nm wavelength laser beam emitted from Verdi-G2 (Coherent, Santa Clara, CA, USA) was utilized, maintaining a low incident power below P = 10 mW to prevent any damage to the sample. The laser spot diameter with a 5× microscope objective was 5 µm. Changes in Brillouin spectra were observed at the central point on laser-heated and ablated chicken skin, corresponding to the temperatures recorded using temperature-sensing fibers.

The ablation process was executed using a fiber-coupled mid-power laser operating continuously (980 nm, Roithner Lasertechnik GmbH, Austria). The laser was calibrated and adjusted to currents of 1 - 2.34 A, equivalent to P = 0.5 - 3.6 W, and each spectral measurement during the ablation procedure lasted 5 minutes. Delivery of the laser light to the skin phantom was achieved through a 1 m long fiber applicator with a core diameter of 400 µm. A holder was used to stabilize the laser applicator at a 45-degree angle relative to the tissue, as illustrated in Fig. 1, facilitating the laser ablation on the tissue surface. Then, a convex lens was utilized to focus an IR-laser beam between two central fibers to an approximate diameter of 1 cm. The thermal ablation adhered to the European protocol of "Tree Rs"29 and was performed on a commercially

Biomedical Optics EXPRESS

obtained chicken skin. Our frozen chicken sample was purchased from a local butcher shop and defrosted by bringing it to a room temperature of 22–25 °C, after which our experiments were performed on a sliced chicken skin sample. The ablation was repeated three times at different areas of the chicken skin sample under the same conditions to determine the average values of spectral width, position and intensity and extract corresponding error bars defined as standard deviation.

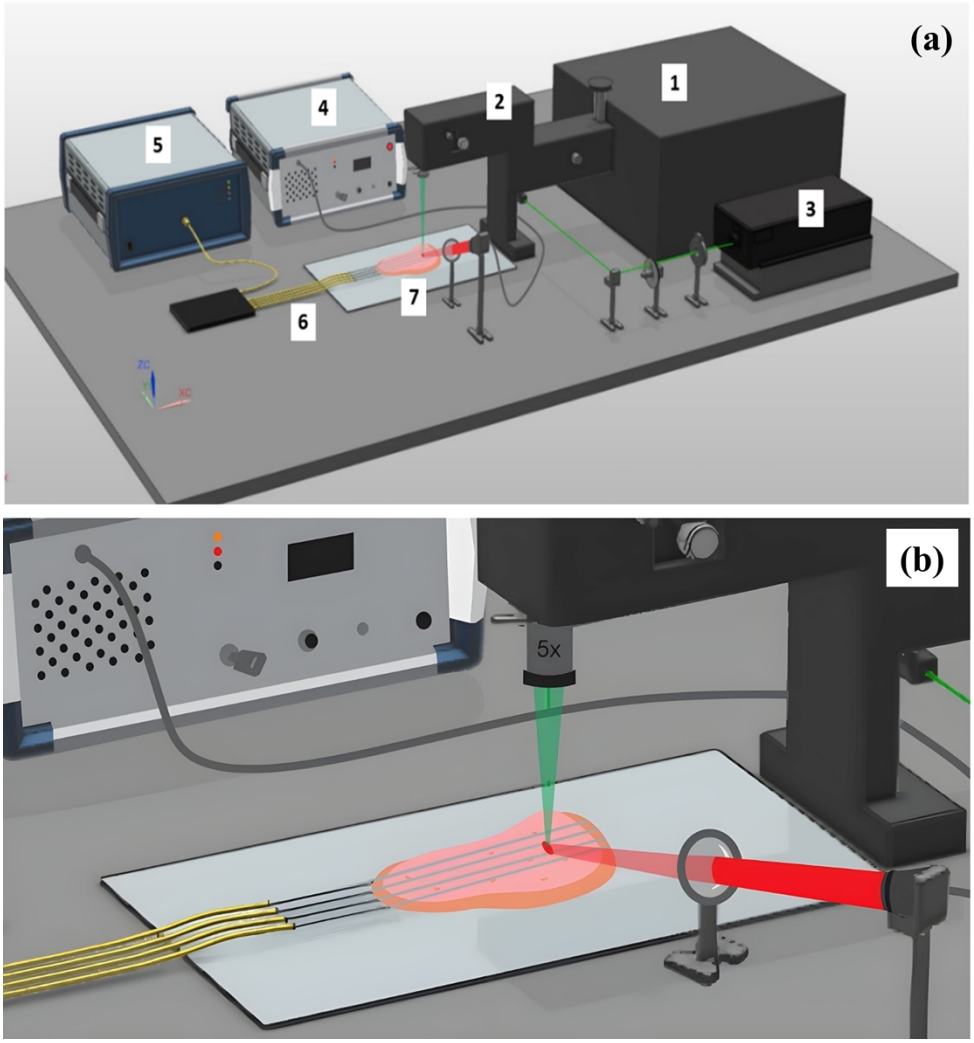

Fig. 1. (a) Assembled Hybrid BLS spectroscopy - OBR thermometry setup. (1) Tandem Fabry–Perot interferometer TFP-2, (2) Confocal microscope, (3) Verdi-G2 532 nm laser source, (4) IR-laser (980 nm) controller, (5) OBR Luna 4600 with a computer used for data acquisition, (6) Optical fibers, (7) Chicken skin. (b) Closer view of the illustration of optical fibers.

The temperature values were acquired by Luna OBR 4600 (Luna Inc., Roanoke, VA, USA), which is capable of detecting backscattered events along the optical fiber during temperature changes (Fig. S1 of Supplement 1 shows the backscattering intensity along the fibers). The OBR was connected to fiber lines that were fitted into the chicken skin. The parameters of the OBR were set as follows: 1. Center Wavelength: 1568.92 nm, 2. Wavelength range: 43.01 nm, 3.

Biomedical Optics EXPRESS

Sensing range: 1.215 m, 4. Sensor spacing: 2 mm. FOSs were placed in parallel to a displayed x-axis of the tissue phantom. The multiplexed position of the FOSs over the ablation area enables monitoring the temperature change for a larger area covering not only the central area, but also the peripheral region of the ablated diameter. In order to obtain the temperature profile above the ablated region, the scattering-level multiplexing (SLMux) configuration was utilized. Beisenova et al. [29] demonstrated the SLMux, a novel system of distributed optical fiber sensors capable of accurately determining the temperature distribution during thermotherapy with a resolution of 2.5 mm. The experiment setup involved SLMux with four parallel lines. These lines were prepared by splicing an SMF-28 separator to a 20 cm length of Nanoparticle-Doped Fiber (NPDF) with high scattering properties. The last 6 centimeters of each NPDF were inserted into the chicken skin with meat at a distance of 0.5 centimeters between them at a room temperature of 20 °C. Consequently, the system achieved a resolution of 5×2 mm or 0.5×0.2 cm, providing 120 sensing points. Considering these specifications, the resulting sensing area measured 6 by 1.5 centimeters, equivalent to 900 square millimeters.

The data collection process was conducted continuously over one hour for each experiment, exploring a range of powers including 0.5, 1.3, 2.0, 2.5, 3.0, and 3.6 W. Approximately 46 measurements were recorded every minute, implying a measurement frequency of roughly 1.3 seconds. This approach resulted in around 3000 measurements for each experiment. Following data collection, the comprehensive dataset underwent analysis using the capabilities of MATLAB. Constructing a 2D map by positioning sensors every 2 mm along the X-axis and optical fibers every 0.5 centimeters along the Y-axis, MATLAB "Curve Fitting Toolbox" were employed for data output. Employing "Cubic spline" interpolation between each sensing point, "Contour" plots were generated, revealing temperature variation levels at intervals of 5 degrees. The observation periods were chosen at time intervals of 1, 2, 5, 10, 15, 20, 30, 40, 50, and 60 minutes. The obtained results were then depicted into corresponding figures, after which tables (Tables S1, S2, S3 are available in Supplement 1) were filled using a photo editing program to define the cytotoxic and ablation area. This involved calculating the pixel to pixel area in the selected temperature level region, and converting this value to square millimeters.

OBR Measured local temperature values were used to validate our 3D FEM simulated of temperature excursions in chicken skin performed using the heat conduction module of the COMSOL Multiphysics 6.1 software. The time-dependent bio-heat conduction equation was solved numerically using the absorption and reflection coefficient at 980 nm laser wavelength through chicken skin. The reflectance spectrum was measured using UV-Vis Spectrometer (Perkin Elmer, Lambda 1050). COMSOL simulation details and the resulting temperature profiles are presented in Figures S8, S9, and S10 of the Supplement 1.

3. Results and discussion

Figure 2 exhibits measured characteristic Brillouin spectra (fitted by Voight function) of chicken skin while heating with a 3.6 W IR-laser power over varying laser irradiation durations. Our BLS measurements, utilizing a backscattering configuration, permitted the assessment of bulk longitudinal acoustic (LA) wave velocity exclusively. At the beginning, the Brillouin peaks experienced a notable increase in intensity, corresponding to water release initiated by the heat. Subsequently, these peaks began diminishing as the tissues underwent complete dehydration caused by the ablation, consequently influencing the elasto-optic coupling. Figure 3 illustrates the two-dimensional thermal maps that elucidate alterations in temperature throughout *the same laser heating and ablation procedure*, specifically under fixed incident laser power of $P = 3.6$ W at different time intervals: 1, 2, 5, 10, 15, 20, 30, 40, 50, and 60 minutes (Thermal maps of other incident laser powers are presented in Figures S2, S3, S4, S5, and S6 of the Supplement 1). These thermal maps were derived through the analysis of data collected along the lengths of all four sensing fibers doped with Mg-silicate-NPs.

Biomedical Optics EXPRESS

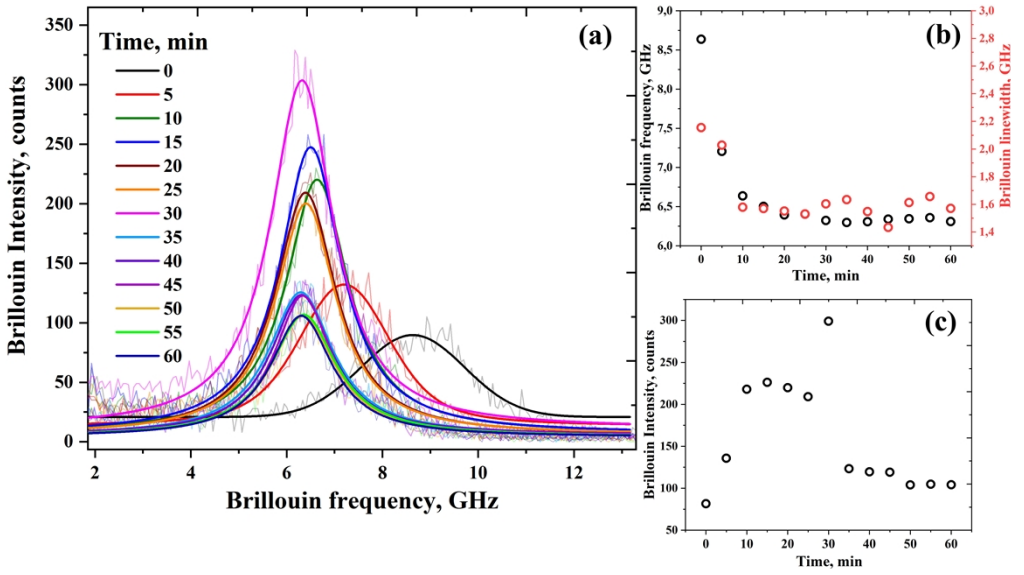

Fig. 2. The time-resolved measured and Voight fitted Brillouin spectra (a), Brillouin frequency and linewidth (b) and Brillouin Intensity (c) values of chicken skin under IR laser heating at 3.6 W.

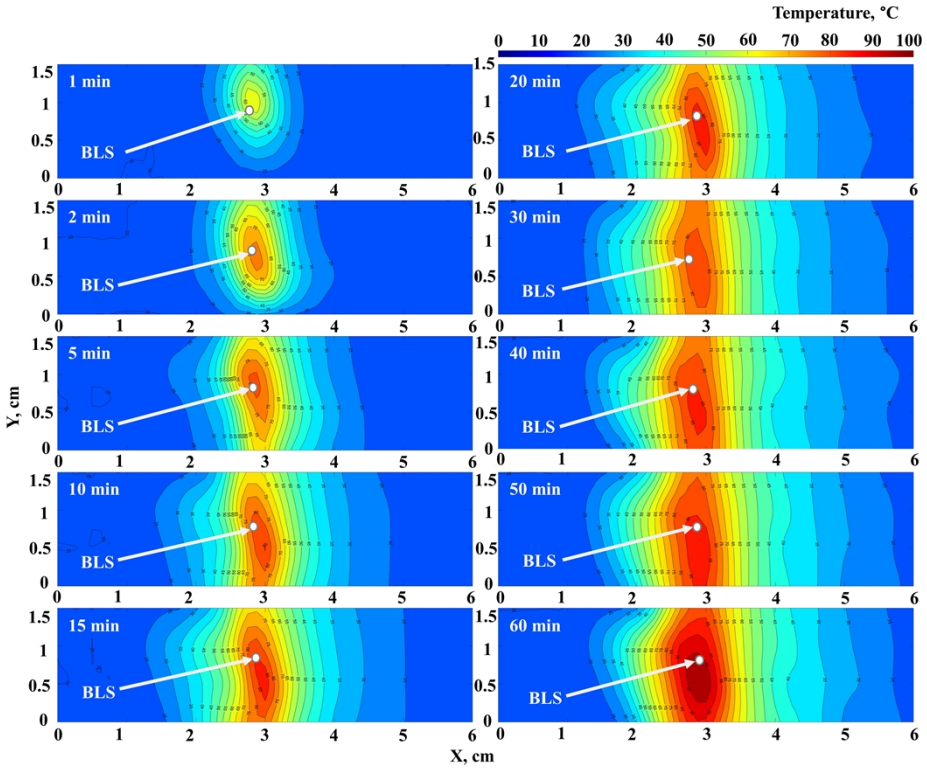

Fig. 3. Typical evolution of spatial surface two-dimensional thermal map measured by OBR on pristine chicken skin during the laser heating and ablation at P = 3.6 W. To guide the eye, the BLS probed region is shown with a white spot on these thermal maps.

Biomedical Optics EXPRESS

In accordance with thermal dosimetry by [36], protein coagulation occurs at T ~ 60 °C, causing nearly rapid cell death. This phenomenon elucidates the thermal threshold beyond which the cellular structures yield to irreversible damage. Conversely, the temperatures T < 42°C are identified as inconsequential in terms of thermal damage, thus relegating the impact of such conditions on cellular viability are minimal. Therefore, T = 42-60°C appears to be a critical temperature range where cellular damage becomes apparent and cellular structures experience partial damage. One important factor to take into account is the duration of heat exposure. The authors [36] provide evidence that cellular death can occur after about one minute at T = 52°C. This highlights the complex interplay between temperature and temporal factors in the context of thermal dosimetry. This clarification emphasizes how therapy modalities must be calibrated carefully to attain the best results possible, balancing the risk of both partial and total cellular damage within the specified temperature range. Considering that the exposure is long, several minutes, we would obtain a quite high mortality rate for most of the cytotoxic temperatures. In the thermal damage identification [37], the temperature > 60 °C provides nearly instantaneous mortality due to the protein coagulation, while the typical condition that clinicians target is the exposure to 52 °C for one minute, which is guaranteed in this paper by a longer ablation time of several minutes. Overall, the thermal damage mortality rate recorded in the experiments would vary only in a narrow temperature range corresponding to the low range of the temperatures (~ 42 - 46 °C, the bottom range of temperature-induced mortality).

Figure 4(a) presents the thermal map of chicken skin exposed to a 3W IR laser, as determined by OBR measurements and FEM simulations. The maps show a close alignment in the maximum temperature (75-76°C) and heating area between the experimental and simulated results. The non-uniform temperature distribution observed in the OBR measurements, in contrast to the FEM simulation, can be attributed to the inherent heterogeneous structure of the chicken tissue. Figure 4(b) demonstrates the rise in temperature over a period, as detected by OBR and simulated using FEM, under different laser power settings. At first, there was a rapid temperature rise over a 10-minute span, followed by a slower temperature increase.

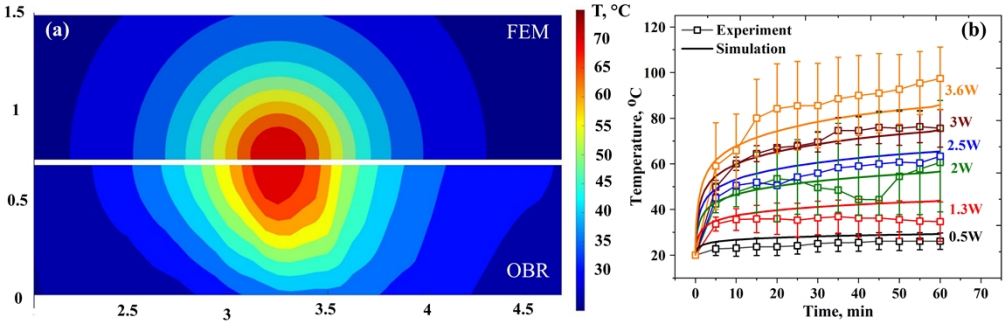

Fig. 4. (a) Temperature sensing map by OBR and FEM simulation for a 3W laser power at 40 minutes of ablation time. (b) The increase in temperature over time, measured using OBR and modeled through FEM, at various laser powers.

The point where the maximum laser-induced temperature was detected, which is at X = 3 cm and Y = 0.5 - 1.0 cm, i.e. p between the second and third sensing fibers, was the target of the laser beam. A peak temperature elevation is clearly visible in the laser targeted zone of the thermal maps and the different colors show how the heat is distributed throughout the tissue.

Figure 5 demonstrates the thermal maps of chicken skin at 30 min laser heating and ablation corresponding to different incident laser powers. These results show laser-induced enhancement of heat-affected zone areas for different incident laser powers applied during the same irradiation duration. The cytotoxic (at T 42°C) and thermally damaged (at T 60°C) areas of chicken skin

Biomedical Optics EXPRESS

under various experimental conditions were introduced in FigS7 of the Supplement 1. The skin, subjected to a high-power IR laser, exhibited a greater extent of thermal heating and ablation compared to the skin treated with a low-power laser.

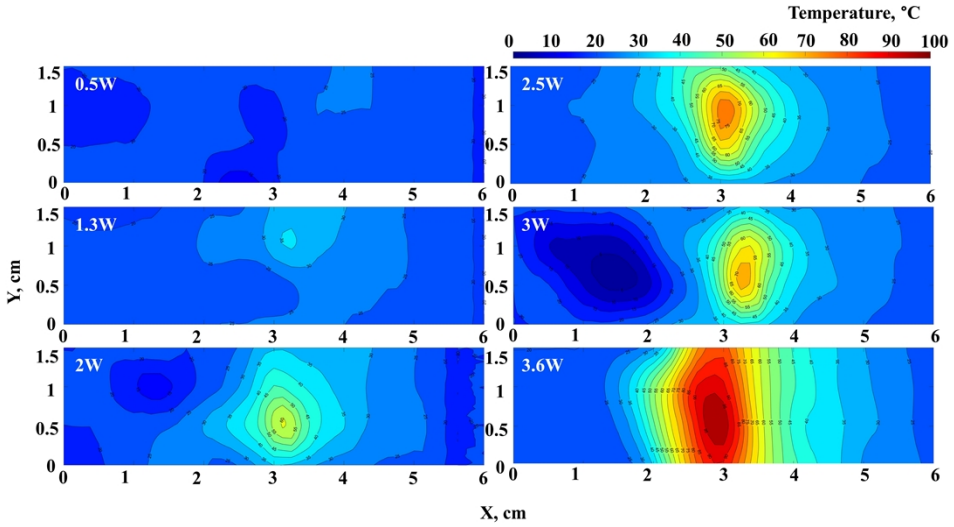

Fig. 5. Two-dimensional thermal map of pristine chicken skin during the laser heating and ablation at the same t = 30 min heating duration for different incident laser powers.

Figures 6(a) and (b) display the spectral Brillouin shift (elastic property) and the linewidths (viscous property), respectively, as a function of laser heating time at different fixed incident laser powers. At low laser powers (0.5, 1.3W), the Brillouin frequency does not change position for the entire duration of the experiment. Starting from higher laser powers (2 - 3.6W), there is a sizeable downshift of the Brillouin peak position during the first 10 minutes of laser irradiation, indicating increased softening of the skin with almost no further softening at longer heating durations (up to 55 min). It should be noted that reduction in stiffness intensifies with the rising of incident laser powers. In contrast, the linewidth shows a slight decrease with increasing laser powers, implying that skin viscosity undergoes slight reduction with the rising laser power (Fig. 7(b)).

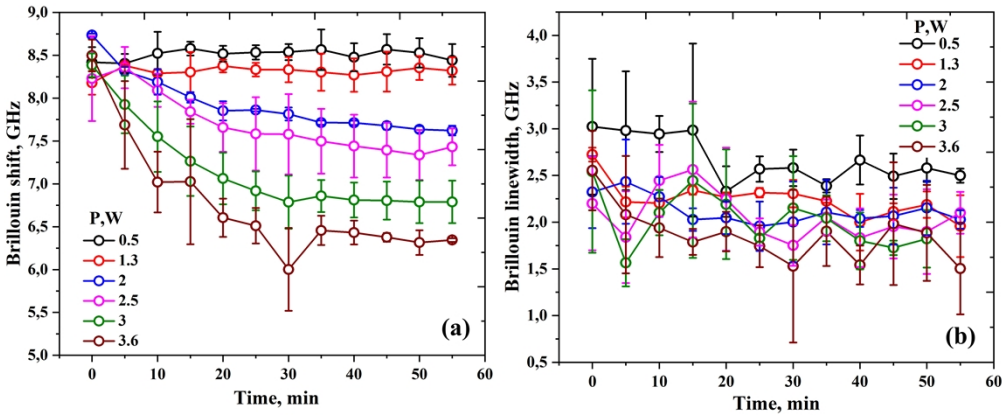

Fig. 6. The Brillouin frequencies (a) and linewidths (b) of chicken skin at different IR-laser powers.

Biomedical Optics EXPRESS

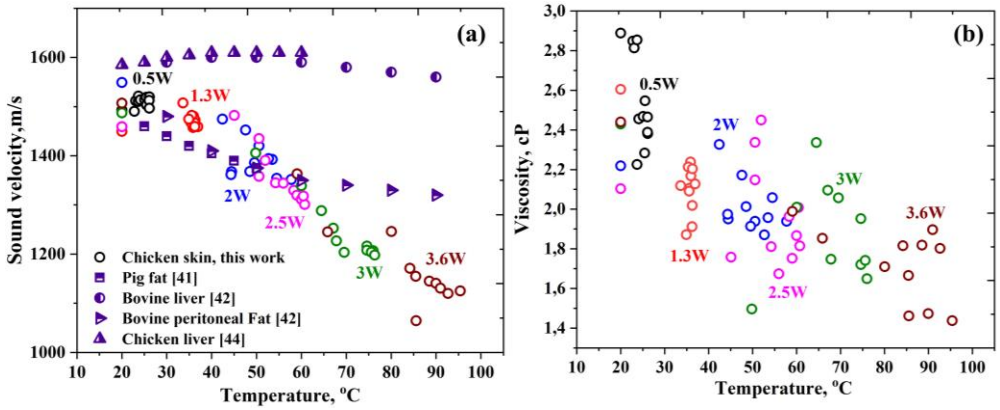

Fig. 7. Temperature-dependent LA velocity V_{LA} (a) and longitudinal viscosity η (b) of chicken skin determined at different incident IR laser powers.

The connection between the frequency shift of Brillouin peaks and the LA (or compressional) sound velocity V_{LA} of the corresponding acoustic mode directly derived as follows [38]:

$$V_{LA} = \frac{\lambda_i \vartheta_L}{2n}, \tag{1}$$

where ϑ_L is the longitudinal acoustic phonon frequency deduced from the Brillouin peak frequency shift; λ_i is the incident light wavelength and n is the refractive index of the skin, taken from the literature [39].

The relation between Brillouin linewidth () and dynamic viscosity is derived by the formula [40]:

$$\Gamma_B = \frac{16\pi^2 n^2}{\rho \lambda_i^2} \left[\eta + \frac{k}{C_p}(\gamma - 1)\right] \tag{2}$$

where ρ - density, κ - thermal conductivity, and γ is the ratio of specific heats (C_p) at constant pressure and volume ($\gamma \sim 1$ for biological tissues). Then the viscosity η is determined by:

$$\eta = \frac{\rho \lambda_i^2}{16\pi^2 n^2} \Gamma_B \tag{3}$$

Using data from time-resolved temperatures (Fig. 4(b)), Brillouin shifts (Fig. 6(a)) and Brillouin linewidths (Fig. 6(b)) all measured at different incident laser powers, present the results of temperature-dependent variation of LA velocity V_{LA} and longitudinal viscosity η in Fig. 7(a) and 7(b), respectively. The V_{LA} in chicken skin decreases with rising temperature. In general, V_L of our chicken skin is in the range of the speed of sound values for other soft tissues and has a similar trend to fatty tissues [41,42]. The chicken skin, which contains 30–40% fat with high levels of n-3 and n-6 fatty acids and 8–12% protein, is a good source of collagen [43]. It is well-known that as temperature increases, acoustic waves travel faster in water-based tissues, whereas the speed of sound decreases in fatty tissues due to the phase transition process of lipids [44,45]. A decrease in viscosity η is notable at high heating rates (high laser powers), while it remains unaltered at low heating rates. This change in viscosity with temperature in our chicken skin is in good agreement with porcine skin and liver samples [10,46]. It is acknowledged that collagen also influences skin tissue's viscoelastic traits and stiffness under quasi-static conditions. This suggests collagen's pivotal role in determining the overall mechanical characteristics of skin

Biomedical Optics EXPRESS

tissue [10]. Unfortunately, we could not find any information on temperature-dependent refractive index (at 532 nm wavelength of the incident laser beam) and density for chicken skin undergoing laser heating. For example, the liver tissue does not undergo substantial change in its density during temperature elevation from room temperature up to 95°C [47]. A slight increase in the refractive index of the cornea (from 1.37 to 1.39) was detected [48] after laser treatment, though the authors did not provide to what maximum temperature laser-induced heating was conducted. In other words, the above listed change in refractive index does not exceed 10% of that at room temperature, which suggests there is a minor effect of heating on longitudinal sound velocity and viscosity values. Therefore, room temperature values [39,49,50] were assumed for determination of viscosities and LA sound velocities at various temperatures. Dynamic mechanical changes stem from both water loss and alterations in the material's intrinsic molecular structure (including lipid phase transition) due to heating. Hence, the intensity, linewidth and frequency variations observed in BLS spectra are attributed to the release of water due to the denaturation of collagen molecules and lipid phase transition during heating.

The experiments were also provided on pig skin as it is closely mimicking the human skin in terms of structure, thickness and collagen content. However, the presence of blood vessels and higher blood content in the pig skin lead to increased optical absorption, potentially reducing the signal quality in BLS measurements. Chicken skin, with its lower blood content, is substantially more transparent than pig skin resulting in higher Brillouin scattering signal due to enhanced elasto-optic interaction associated with larger scattering volume within optically probed bulk longitudinal acoustic waves inside chicken skin.

Figures 8(a) and (b) we show observed the changes of Brillouin frequency and linewidth, LA velocity V_{LA} and longitudinal viscosity η before, during and after heating of chicken skin at an incident IR laser power of P = 2W. However, right after IR laser heating was stopped, the Brillouin linewidth (i.e. viscosity) remained unaltered, while there was significant increase in the Brillouin shift frequency during this cooling of the tissue back to room temperature, as shown in the figure below. But the Brillouin shift did not recover fully back to its pre-heating value. This post-heating, cooling-driven stiffening of the tissue is an interesting phenomenon which needs to be systematically studied as a function of incident IR laser power and temperature to closely monitor mechanical variation of tissues and relate them to expected physiological changes such as protein denaturation and cell damage. This is beyond the scope of current study and is the subject of future investigation.

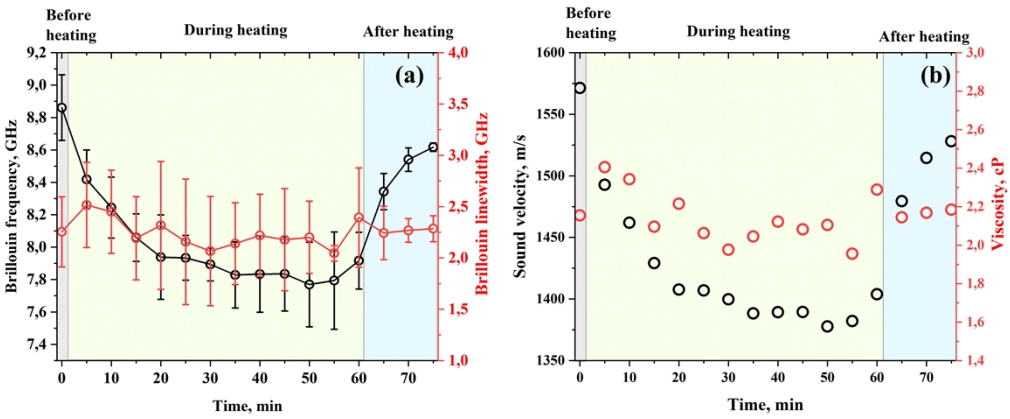

Fig. 8. Time-dependent Brillouin frequency and linewidth (a), LA velocity V_{LA} and longitudinal viscosity η (b) change of chicken skin before, during and after heating at an incident IR laser power of P = 2W.

Biomedical Optics EXPRESS

4. Conclusion

In summary, we conducted for the first time real-time, *in-situ* hybrid measurements of local visco-elastic properties and surface temperature of chicken skin using BLS spectroscopy and OBR with Mg-silica-NP doped fibers, respectively, during laser-induced heating and ablation. OBR-measured spatial temperature distributions at various IR laser heating powers were employed to validate local temperature variations modeled by the finite element meshing (FEM) method, solving Pennes' bio-heat transfer equation. Substantial reduction in skin tissue stiffness and slight decrease in its viscosity is associated with water loss and heat-induced structural modifications during the laser-driven heating and ablation processes. These findings pave the way for simultaneous real-time hybrid optical sensing of viscoelasticity and local temperature in biological tissues experiencing denaturation and gelation during thermal ablation in clinical settings. The real-time capability of the hybrid visco-elasto-thermometric approach could be applied to "smart" therapeutic ablation of superficial tissues, such as in the treatment of bladder carcinomas, non-melanoma skin cancers, or breast carcinoma with their thermo-mechanical properties informed in real-time during diagnostics and hyperthermic surgeries.

Funding. Nazarbayev University (091019CRP2105, 201223FD8806).

Acknowledgments. The authors acknowledge the funding from the Nazarbayev University Collaborative Research Program (CRP) Grant (091019CRP2105) and from Faculty Development Competitive Research program (FDCRGP) Grant (201223FD8806).

Disclosures. The authors declare no conflict of interest.

Data availability. The raw data required to reproduce these findings are available from the corresponding author, upon email request. The processed data required to reproduce these findings are also available upon request.

Supplemental document. See Supplement 1 for supporting content.

References

1. M. Ghanbari and G. Rezazadeh, "Thermo-vibrational analyses of skin tissue subjected to laser heating source in thermal therapy," Sci. Rep. **11**(1), 22633 (2021).
2. X. Li, Y. Zhong, R. Jazar, *et al.*, "Thermal-mechanical deformation modeling of soft tissues for thermal ablation," Bio-Med. Mater. Eng. **24**(6), 2299–2310 (2014).
3. O. Ashraf, N. V. Patel, S. Hanf, *et al.*, "Laser-induced thermal therapy in neuro-oncology: a review," World Neurosurg. **112**, 166–177 (2018).
4. R. J. Staford, D. Fuentes, A. A. Elliott, *et al.*, "Laser-induced thermal therapy for tumor ablation," Crit. Rev. Biomed. Eng. **38**, 79–100 (2010).
5. M. Riordan and Z. Tovar-Spinoza, "Laser-induced thermal therapy (LITT) for pediatric brain tumors: case-based review," Transl. Pediatr. **3**(3), 229–235 (2014).
6. S. V. Esser, G. Stapper, P. J. V. Diest, *et al.*, "Ultrasound-guided laser-induced thermal therapy for small palpable invasive breast carcinomas: a feasibility study," Ann. Surg. Oncol. **16**(8), 2259–2263 (2009).
7. K. S. Shibib, M. A. Munshid, and H. A. Lateef, "The effect of laser power, blood perfusion, thermal and optical properties of human liver tissue on thermal damage in LITT," Lasers Med. Sci. **32**(9), 2039–2046 (2017).
8. A. Zhang, J. Wang, and B. Wang, "Bio-thermo-viscoelastic behavior in multilayer skin tissue," Journal of Thermal Stresses **45**(7), 559–575 (2022).
9. F. Xu, T. J. Lu, and K. A. Seffen, "Biothermomechanics of skin tissues," J. Mech. Phys. Solids **56**(5), 1852–1884 (2008).
10. F. Xu, K. A. Seffen, and T. J. Lu, "Temperature-dependent mechanical behaviors of skin tissue," International Journal of Computer Science **35**(1), 92–101 (2007).
11. A. Ezzat, "The relaxation effects of the volume properties of electrically conducting viscoelastic material," J. Mater. Sci. Eng. B **130**(1-3), 11–23 (2006).
12. Y. Chae, G. Aguilar, E. J. Lavernia, *et al.*, "Characterization of temperature dependent mechanical behaviour of cartilage," Lasers Surg. Med. **32**(4), 271–278 (2003).
13. J. F. Mano, "Viscoelastic properties of bone: Mechanical spectroscopy studies on a chicken model," Mater. Sci. Eng., C **25**(2), 145–152 (2005).
14. C. Li, J. Huang, K. L. Wang, *et al.*, "Investigation on thermal damage model of skin tissue in vitro by infrared laser welding," Opt. Laser. Eng. **124**, 105807 (2020).
15. Z. L. Deng and J. Liu, "Analytical study on bioheat transfer problems with spatial or transient heating on skin surface or inside biological bodies," J. Biomech. Eng. **124**(6), 638–649 (2002).

Biomedical Optics EXPRESS

16. X. Li, Q. H. Qin, and X. Tian, "Thermo-viscoelastic analysis of biological tissue during hyperthermia treatment," Appl. Math. Model. **79**, 881–895 (2020).
17. F. S. Alzahrania and I. A. Abbas, "Analytical estimations of temperature in a living tissue generated by laser irradiation using experimental data," J. Therm. Biol. **85**, 102421 (2019).
18. D. Fioretto and F. Scarponi, "Dynamics of a glassy polymer studied by Brillouin light scattering," Mater. Sci. Eng. A **521-522**, 243–246 (2009).
19. N. Almas, B. Kurbanova, N. Zhakiyev, *et al.*, "Mechano-chemical properties of electron beam irradiated polyetheretherketone," Polymers **14**(15), 3067 (2022).
20. S. Speziale, H. Marquardt, and T. S. Duffy, "Brillouin scattering and its application in geosciences," Rev. Mineral. Geochem. **78**(1), 543–603 (2014).
21. D. Akilbekova, V. Ogay, T. Yakupov, *et al.*, "Brillouin spectroscopy and radiography for assessment of viscoelastic and regenerative properties of mammalian bones," J. Biomed. Opt. **23**(09), 1 (2018).
22. A. Rakymzhan, T. Yakupov, Z. Yelemessova, *et al.*, "Time-resolved assessment of drying plants by Brillouin and Raman spectroscopies," J. Raman Spectrosc. **50**(12), 1881–1889 (2019).
23. Z. Coker, M. Troyanova-Wood, A. J. Traverso, *et al.*, "Assessing performance of modern Brillouin spectrometers," Opt. Express **26**(3), 2400–2409 (2018).
24. A. Gaipov, Z. Utegulov, R. Bukasov, *et al.*, "Development and validation of hybrid Brillouin-Raman spectroscopy for non-contact assessment of mechano chemical properties of urine proteins as biomarkers of kidney diseases," BMC Nephrol. **21**(1), 229 (2020).
25. C. H. Kharmyssov, Z. H. Nurekeyev, A. Gaipov, *et al.*, "Mechano-chemistry across phase transitions in heated albumin protein solutions," Polymers **15**(9), 2039 (2023).
26. C. H. Kharmyssov and Z. N. Utegulov, "Brillouin biosensing of viscoelasticity across phase transitions in ovine cornea," Biosensors **14**(8), 371 (2024).
27. G. Antonacci and S. Braakman, "Biomechanics of subcellular structures by non-invasive Brillouin microscopy," Sci. Rep. **6**(1), 37217 (2016).
28. K. Elsayad, S. Werner, M. Gallemi, *et al.*, "Mapping the subcellular mechanical properties of live cells in tissues with fluorescence emission–Brillouin imaging," Sci. Signal. **9**(435), rs5 (2016).
29. A. Beisenova, A. Issatayeva, S. Sovetov, *et al.*, "Multi-fiber distributed thermal profiling of minimally invasive thermal ablation with scattering-level multi plexing in MgO-doped fibers," Biomed. Opt. Express **10**(3), 1282–1296 (2019).
30. H. Martines-Arano, S. Palacios-Barreto, J. Castillo-Cruz, *et al.*, "Fractional photodamage triggered by chaotic attractors in human lung epithelial cancer cells," Int. J. Therm. Sci. **181**, 107734 (2022).
31. B. Kurbanova, Z. Ashikbayeva, A. Amantayeva, *et al.*, "Thermo-Visco-Elastometry of RF-Wave-Heated and Ablated Flesh Tissues Containing Au Nanoparticles," Biosensors **13**(1), 8 (2022).
32. P. R. Stauffer, "Thermal therapy techniques for skin and superficial tissue disease. In Matching the energy source to the clinical need: a critical review," SPIE Proceedings 321–361 (2000).
33. H. A. Syed, C. S. Biyani, N. Bryan, *et al.*, "Holmium:YAG laser treatment of recurrent superficial bladder carcinoma: Initial clinical experience," J. Endourol. **15**(6), 141–151 (2004).
34. E. S. Marmur, C. D. Schmults, and D. J. Goldberg, "A review of laser and photodynamic therapy for the treatment of nonmelanoma skin cancer," Dermatol. Surg. **30**, 264–271 (2004).
35. H. H. Pennes, "Analysis of tissue and arterial blood temperatures in the resting human forearm," J. Appl. Physiol. **1**(2), 93–122 (1948).
36. S. Sapareto and W. Dewey, "Thermal dose determination in cancer therapy," Int. J. Radiat. Oncol., Biol., Phys. **10**(6), 787–800 (1984).
37. H. Rhim, S.N. Goldberg, G.D. Dodd, *et al.*, "Essential techniques for successful radio-frequency thermal ablation of malignant hepatic tumors," Radiographics **21**(suppl_1), S17–S35 (2001).
38. L. L. Stevens, E. B. Orler, D. M. Dattelbaum, *et al.*, "Brillouin-scattering determination of the acoustic properties and their pressure dependence for three polymeric elastomers," J. Chem. Phys. **127**(10), 104906 (2007).
39. R. Khan, B. Gul, S. Khan, *et al.*, "Refractive index of biological tissues: Review, measurement techniques, and applications," Photodiagn. Photodyn. Ther. **33**, 102192 (2021).
40. S. H. Chen, C. C. Lai, and J. Rouch, "Experimental confirmation of renormalization - group prediction of critical concentration fluctuation rate in hydrodynamic limit," J Chem Phys **68**(4), 1994–1995 (1978).
41. S. A. López-Haro, L. Leija, L. Favari, *et al.*, "Measurement of ultrasonic properties into biological tissues in the hyperthermia temperature range," Phys. Procedia **3**(1), 551–558 (2010).
42. J. C. Bamber and C. R. Hill, "Ultrasonic attenuation and propagation speed in mammalian tissues as a function of temperature," Ultrasound Med. Biol. **5**(2), 149–157 (1979).
43. N. Ibarz-Blanch, J. M. Alcaide-Hidalgo, A. J. Cortes-Espinar, *et al.*, "Chicken slaughterhouse by-products: A source of protein hydrolysates to manage non-communicable diseases," Trends Food Sci. Technol. **139**, 104125 (2023).
44. R. Martínez-Valdez, V. H. M. Contreras, A. Vera, *et al.*, "Sound speed measurement of chicken liver from 22°C to 60°C," Phys. Procedia **70**, 1260–1263 (2015).
45. I. Y. Yanina, E. N. Lazareva, and V. V. Tuchin, "Refractive index of adipose tissue and lipid droplet measured in wide spectral and temperature ranges," Appl. Opt. **57**(17), 4839–4848 (2018).

Biomedical Optics EXPRESS

46. C. Wex, S. Arndt, K. Brandstadter, *et al.*, "Biomechanical characterization of material properties of porcine liver after thermal treatment," Soft Mater. **12**(4), 411–419 (2014).
47. N. P. Silva, A. Bottiglieri, R. C. Conceicao, *et al.*, "Characterisation of ex vivo liver thermal properties for electromagnetic-based hyper thermic therapies," Sensors **20**(10), 3004 (2020).
48. S. Patel, L. A. Jorge, and A. Artola, "Changes in the refractive index of the human corneal stroma during laser in situ keratomileusis. Effects of exposure time and method used to create the flap," J. Cataract Refract Surg. **34**(7), 1077–1082 (2008).
49. M. Fu, W. Weng, and H. Yuan, "Numerical simulation of the effects of blood perfusion, water diffusion, and vaporization on the skin temperature and burn injuries," Numer. Heat Transfer, Part A **65**(12), 1187–1203 (2014).
50. T. Kono and J. Yamada, "In vivo measurement of optical properties of human skin for 450–800 nm and 950–1600 nm wavelengths," Int. J. Thermophys. **40**(5), 51 (2019).